Nanostructure diffusion and aggregation on desorbing rare-gas solids: Slip on an incommensurate lattice

V. N. Antonov, J. S. Palmer, A. S. Bhatti,* and J. H. Weaver
Department of Physics, Department of Materials Science and Engineering, and Frederick Seitz Materials Research Laboratory, University of Illinois at Urbana-Champaign, Urbana, Illinois 61801, USA
(Received 16 June 2003; published 20 November 2003)

Physical vapor deposition of a wide range of materials on rare-gas solids leads to spontaneous cluster formation. Desorption of the rare-gas buffer causes the clusters to aggregate, a process known as buffer-layer-assisted growth. We have studied the extent of aggregation and the size distribution of Au nanostructures as a function of the buffer composition (Xe, Kr, and Ar) and thickness, using transmission electron microscopy to image them after buffer desorption and delivery to amorphous carbon substrates. For small compact Au nanostructures (less than ~ 5 nm mean radius, $\leqslant 3\times 10^4$ atoms), the diffusivity varies strongly with size and even increases with average size in a limited range. This enhanced diffusion phenomenon is attributed to self-heating during coalescence. It is most important for small particles and is more evident on Kr than on Xe because of weaker interface coupling. In the limit of large ramified Au nanostructures (exceeding ~ 10 nm mean radius, $\geqslant 2\times 10^5$ atoms), the diffusivity scales as the inverse of the contact area, in agreement with molecular dynamics simulations of fast slip diffusion of nanocrystals on incommensurate surfaces. Motion is driven by phonons of the cluster and substrate, and is controlled by friction between a cluster facet and the buffer surface. A simple model is proposed that explains the observed exponential dependence of cluster size on buffer thickness. In this model, the growth kinetics are controlled by competition between the rate of cluster diffusion and the rate of buffer depletion.

DOI: 10.1103/PhysRevB.68.205418 PACS number(s): 61.46.+w, 36.40.Sx, 68.65.−k, 68.35.Af

I. INTRODUCTION

The drive to produce nanostructures with tailor-made properties has been accompanied by experimental and theoretical studies of self-assembly processes.[1] Huang *et al.*[2] introduced a particularly interesting self-assembly technique known as buffer-layer-assisted growth (BLAG), following earlier work by Waddill *et al.*[3,4] In BLAG, atoms are vapor-deposited onto thin layers of rare-gas solids that have been grown at 20–50 K on a substrate of choice.[5] Clusters form spontaneously due to weak bonding with the buffer. Subsequent warm-up activates cluster diffusion, aggregation, and coalescence on the subliming buffer layer. In this way, preformed metal or nonmetal nanostructures establish contact by soft landing on a pristine surface. Their interactions with the surface can then be examined and their intrinsic properties can be explored.

BLAG was initially utilized for fabricating atomically smooth metal-semiconductor junctions in studies of Schottky barrier formation.[4,6] Subsequently, it was discovered that the average size of the produced nanostructures could be varied over more than two orders of magnitude by suitable choice of buffer layer thickness.[2] More recently, it was shown that the fractal dimension of ramified islands formed by BLAG is consistent with Monte Carlo simulations of diffusion-limited cluster-cluster aggregation.[7] This suggests that the clusters experience random, or Brownian, motion. It has also been demonstrated that the BLAG process is not unique to rare-gas solids, as long as the interaction between the buffer and clusters is weak.[8]

In this paper, we focus on the physical origin of BLAG by studying the growth of Au nanostructures on solid Ar, Kr, and Xe on amorphous carbon substrates. Using transmission electron microscopy (TEM) to quantify the cluster density and size distribution, we first demonstrate that the initial nucleation density is independent of buffer thickness, for buffers that completely cover the substrate. Thus, subsequent processes that include diffusion and coalescence commence from the same initial density. We then examine the cluster size distributions for different thicknesses of Ar, Kr, and Xe and amounts of Au. Finally, we compare these results with existing models and simulations that describe the kinetics of diffusion-limited particle aggregation.

The diffusivity of small compact Au clusters (mean radius less than ~ 5 nm, corresponding to as many as $\sim 3\times 10^4$ atoms) varies significantly with their size. We attribute this dependence to processes associated with the release of energy as clusters coalesce. This provides extra activation for diffusion. In the large-size limit (mean radius exceeding ~ 10 nm, branched structures, more than $\sim 2\times 10^5$ atoms), the diffusivity scales as the inverse of the contact area with the rare gas surface, consistent with simulations of fast slip diffusion on incommensurate surfaces.[9] Such scaling suggests that the diffusivity is controlled by viscous friction between the buffer and nanocrystal, an interesting example of friction at the nanoscale. Based on these results, we propose a model for BLAG in which the observed particle densities depend on competition between the cluster diffusivity and the rate of buffer desorption (which dictates the amount of time available for diffusion). The model does not include self-heating due to coalescence, and it overestimates the diffusion barrier. Nevertheless, it demonstrates the observed power law dependence of cluster density on buffer layer thickness. These findings bring a deeper understanding of the process of BLAG and diffusion on incommensurate lattices.

II. EXPERIMENT

The samples were grown in an ultrahigh-vacuum chamber with a typical base pressure $<2\times10^{-10}$ Torr. The substrates were 20–30-nm-thick amorphous carbon films suspended on copper grids. Cooling to 20 K was done with a closed-cycle helium refrigerator. Growth of the buffer layers occurred when Ar, Kr, or Xe gas was introduced into the chamber to raise the pressure to 1×10^{-6} Torr. Pressure was monitored with an ion gauge, corrected for each gas sensitivity. The buffer growth rate was estimated from the number of incident atoms per unit time per unit area—namely, $I=p/(2\pi mkT)^{1/2}$, where p is the partial pressure, m is the atomic mass, k is the Boltzmann constant, T is ambient temperature,[10] and the sticking coefficient was assumed to be unity. Following buffer deposition, Au was evaporated from a resistively heated W basket 0.5 m away from the sample. The impinging Au atoms were sufficiently mobile that they formed clusters, as depicted in Fig. 1, a process made possible by the weak bonding with the rare-gas solid. Though the nominal temperature was ~20 K, atom capture by growing clusters released ~3.8 eV/atom (the cohesive energy of Au), and this facilitated compact nanostructure growth. Mobility and aggregation of small clusters during material deposition is also to be expected, contributing significantly to the shape of the size distribution after deposition.[11] As pointed out below, however, the exact shape does not affect the analysis in this study. Desorption of the buffer occurred when the refrigerator was turned off, and this led to cluster aggregation.

After growth, the samples were transferred to a Philips CM12 120-kV transmission electron microscope for characterization. TEM imaging was done in the bright-field mode. The intensity of the beam was low enough not to induce any significant changes in nanostructure morphology. The Au nanostructures were stable on the *a*-carbon substrate, and samples stored in air for more than a year showed no observable changes in cluster size or density.

In this paper, we focus on number densities and particle sizes as a function of the amount of Au deposited and the choice and thickness of the buffer layer. The projected areas and the total number of nanostructures in a given area were obtained directly from the TEM micrographs. The average radius r of a given particle was calculated as the average distance from its center of mass to the perimeter of its projection. Size distribution histograms were obtained by counting how many particles fell within a certain range of average radii or projected areas.

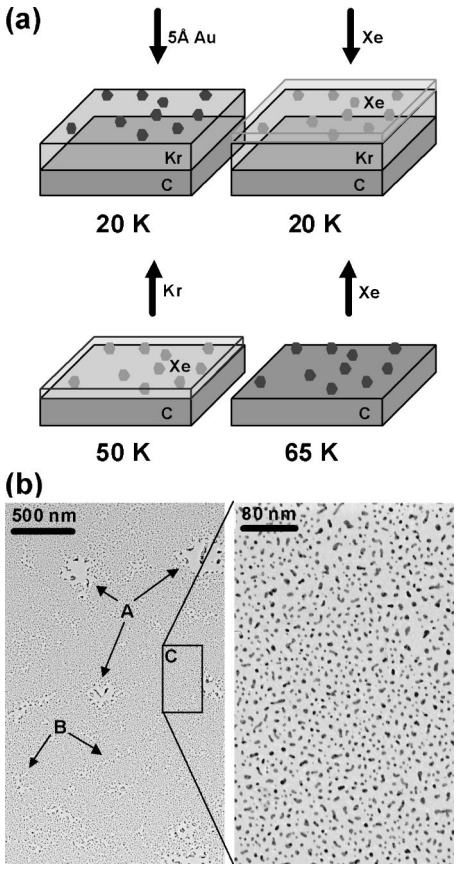

FIG. 1. (a) Depiction of sample preparation involving rare-gas solid buffer condensation at 20 K on amorphous carbon foils for TEM. The upper left indicates 5 Å of Au deposited on a Kr layer. Krypton desorption would lead to particle aggregation before delivery to the surface, as in most of the experiments described here. The other three sketches depict the consequences of a Xe capping layer over the Au clusters. During warm-up of this sandwich structure, Kr desorbs at ~50 K, escaping through the cap while the cap prevents significant lateral motion of the clusters. The residual Xe desorbs above ~60 K, after the Au clusters are already immobilized on the substrate. (b) TEM image showing Au clusters grown on 140 ML Kr with an 8 ML Xe cap. Area *C* is representative of most of the image. In it, the cluster density is equal to that obtained following 5 Å Au deposition on 4 ML buffers—namely, 6×10^{11} cm^{-2}. This shows that the initial nucleation density is independent of the buffer thickness. Areas like *A* and *B* reflect large scale imperfections in the Ar/Xe sandwich and grain boundaries in the capping layer.

III. RESULTS AND DISCUSSION

A. Initial cluster densities

Huang *et al.* showed[2] that the minimum thickness of a Xe buffer needed to provide for clustering and to cover the substrate is ~4 ML (monolayers) and that the final density of clusters delivered to the substrate depends on the buffer layer thickness. Using *in situ* scanning tunneling microscopy, they deduced a density of 5×10^{11} cm^{-2} for 0.1 Å of Ag grown on 4 ML Xe on Si(111)-7×7. When the buffer layer was 60 ML, the density on Si(111) decreased to 2×10^{10} cm^{-2}. An implicit assumption in their discussion of desorption-assisted coalescence was that the cluster nucleation density was independent of the buffer layer thickness. It is important to verify this assumption before undertaking quantitative analyses of cluster diffusivity.

We reasoned that clusters formed on a buffer layer would be frozen in place if they were overcoated by a second rare-gas solid, which would remain solid during buffer desorption. The top right panel of Fig. 1(a) depicts this sandwich structure with Au particles captured between Kr and a cap of Xe. To produce such a sandwich, we deposited 5 Å of Au on 140 ML Kr and capped it with 8 ML of Xe. During warm-up,

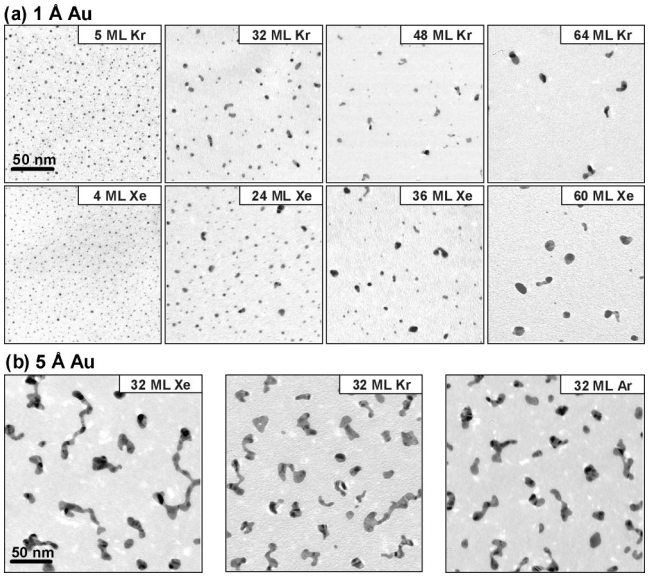

FIG. 2. TEM micrographs of (a) 1 Å Au depositions on buffers of Kr and Xe and (b) 5 Å Au on 32 ML of Xe, Kr, and Ar. Buffer desorption caused cluster motion that led to aggregation. Kr and Ar buffers produced almost identical densities at the same thickness. The lower density for Xe indicates greater cluster diffusivity. The compact clusters in (a) indicate 3D coalescence while the ramified features in (b) indicate 2D growth.

the Kr desorbed completely by 50 K [lower panel Fig. 1(a)] but Xe sublimation became significant only above 60 K, as determined by quadrupole mass spectrometry of the gases in the chamber.

Figure 1(b) is a TEM micrograph of Au clusters on *a*-carbon. As expected, the density is not uniform since Kr escape through the cap is not as simple as depicted. Areas like *A* have low densities, corresponding to extensive cluster aggregation. In them, defects in the carbon film or dust particle contamination were common. (The carbon films were removed from their shipping container and attached to the cold head in the laboratory environment, not a clean room.) Areas like *B* represent a connected network derived from clusters of somewhat higher density. These networks likely reflect areas where crystallites of the Xe cap formed large-angle grain boundaries (characteristic grain size 0.3 μm) and weak links. The important aspect of Fig. 1(b) is that there are large areas like *C* with high uniformity and a density of 6×10^{11} cm^{-2}. As a reference, we formed clusters on buffer layers of minimal thickness where there would be negligible aggregation during desorption. In this case, the density was $(6\pm1)\times10^{11}$ cm^{-2}, and it was independent of the buffer species. We conclude that the initial density is independent of the buffer thickness, at least up to 140 ML of Kr.

B. Nanostructure sizes and morphology

Figure 2 provides representative TEM micrographs from which nanostructure sizes and densities were measured. For Fig. 2(a), the amount of Au deposited was 1 Å, the buffer layer was Kr or Xe, and the images emphasize the dependence of cluster size and density on buffer layer thickness. For 5 ML Kr, the nanostructures were compact and roughly equiaxed. Higher-resolution images showed that they were largely single crystalline with twins.[13] A typical structure formed on 5 ML was faceted and had a characteristic dimension of 2 nm. It would contain ~300 atoms. The density decreased from 1.6×10^{12} for 5 ML to 2×10^{11} cm^{-2} for 32 ML Kr. By 64 ML, the density was 2×10^{10} cm^{-2}, and the structures were less compact.

Growth on Xe produced a similar trend of reduced density and the onset of branched growth with increased buffer thickness. The tendency to branch continued for thicker buffer layers, and it is more apparent for greater amounts of Au. As described by Antonov and Weaver,[8] the transition from compact to ramified structures reflects competition between the arrival rate of new particles and the time needed to coalesce.

Figure 2(b) emphasizes the dependence of BLAG on buffer layer composition with 5 Å of Au deposited onto 32 ML Xe, Kr, and Ar. In all cases, ramified nanostructures were formed. The trend of increased size with buffer thickness was always observed, but the rate of increase depended on the buffer composition. The densities were always higher on Kr and Ar than on Xe layers of a given thickness. Differences reflect the cluster diffusivity and the rates of temperature increase during warm-up, as discussed below in detail.

When considering diffusion, it is important to recognize that the particles are faceted crystals in contact with {111}-textured rare-gas solids and that the lattices are highly incommensurate.[12] High-resolution TEM studies[13] have shown that Au particles of a few nm dimension are {111} faceted with {100} truncations that amount to ~10% of the surface area, as in Fig. 3(a). Figure 3(b) emphasizes the structural consequences of the 51% lattice mismatch for Au(111) on Xe(111). The mismatch is smaller but still very large for Kr (39%) and Ar (31%). This has significant implications for heat dissipation and interface friction, as the effective potential in which the center of mass moves would be very small.[14]

Figure 3(a) depicts coalescence of two crystals that have a characteristic dimension of 4 nm and are made up of ~2000 atoms. Following contact on Xe, there would be rapid reorientation to establish a favorable interface, as shown by simulations.[15,16] The two particles in Fig. 3(a) are shown at the right to have completely coalesced. In the literature, models of coalescence have assumed that the driving force is the radius of curvature of the particles,[17,18] but agreement with simulations has been poor.[16] More realistic models should take into account the crystal structure, as in Fig. 3, to describe atom diffusion on terraces and transfer over edges and steps. Such processes are thermally activated, but the relevant temperature is determined by the energy release upon coalescence and its dissipation through the substrate.

C. Power law dependence of cluster density on buffer thickness

The evolution of the cluster number density $\langle n \rangle$ as a function of buffer thickness is summarized in Fig. 4. Though the initial density does not depend on buffer material, it does

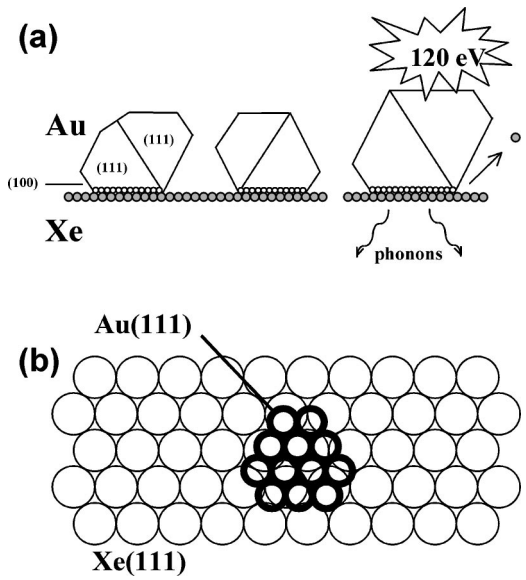

FIG. 3. (a) Au nanocrystals depicted as truncated cubo-octahedrons with dominant {111} facets on a Xe buffer (Ref. 13). Complete coalescence of two such particles, each 4 nm across and derived from ~2000 atoms, releases ~120 eV. This heats the structure assists in restructuring and causes Xe desorption. It also contributes significantly to nanocrystal mobility. The heat is dissipated by phonons. (b) Sketch of the highly incommensurate contact of Au(111) with Xe(111). The lattice mismatch provides a low-friction interface with poor phonon coupling.

depend on the amount of material deposited. For example, $\langle n\rangle = 2\times 10^{12}$ for 1 Å and 6×10^{11} cm^{-2} for 5 Å Au.[19] From Fig. 4, a power law dependence on the buffer thickness θ,

$$\langle n\rangle \propto \theta^{z}, \tag{1}$$

then develops as the thickness increases beyond a critical level, which depends on both coverage and buffer material. Haley and Weaver showed that power law behavior was consistent with Monte Carlo simulations of diffusion-limited cluster-cluster aggregation.[7] Significantly, the power z is nearly the same for 5 Å Au on Xe, Kr, and Ar—namely, -2.31 ± 0.14, -2.28 ± 0.18, and -2.38 ± 0.14, respectively. For 1 Å Au on Xe and Kr, the values are again close, -3.12 ± 0.21 and -3.27 ± 0.14, yet consistently higher than those for 5 Å . We conclude that the slopes in Fig. 4 reflect the details of diffusion of the nanostructures rather than specifics related to the buffer layer makeup. This power law behavior will be used below to deduce upper limits to the activation energy for cluster diffusion.

When considering the difference in the rate of growth for 1 Å and 5 Å Au (Fig. 4), it is important to emphasize that they represent three-dimensional (3D) and 2D coalescence, respectively. In 3D or complete coalescence, two spherical particles of radii r_1 and r_2 merge into a new spherical particle of radius $(r_1^3+r_2^3)^{1/3}$. (BLAG particles are faceted nanocrystals, but this does not affect the generality of the argument.) The surface coverage then decreases and the height of the structures increases. In 2D growth, particles connect without significant rearrangement of material, and

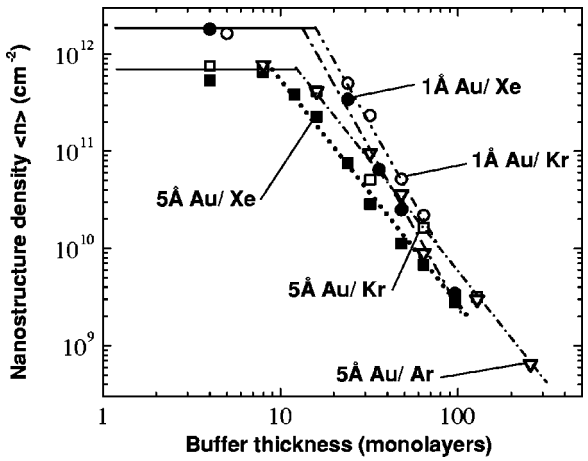

FIG. 4. Nanostructure densities as a function of buffer thickness for 5 Å Au depositions on Xe, Kr, and Ar and for 1 Å Au depositions on Xe and Kr. Power law growth is established after a critical buffer thickness. The power is approximately the same for all 5 Å depositions, reflecting 2D growth with $\langle n\rangle \propto \theta^{-2.3}$. For 1 Å depositions, it corresponds to 3D growth with $\langle n\rangle \propto \theta^{-3.2}$.

the average island height remains constant. Complete coalescence is evident for 1 Å Au on thin layers of Kr and Xe in Fig. 2(a). As the coalescence rate depends strongly on particle size,[17,18] the nanostructure shapes will resemble those of 5 Å Au in Fig. 2(b) for suitably thick buffers.

It is instructive to compare the observed power law dependence with predictions of theoretical models for particle aggregation in the 3D and 2D regimes. Kashchiev developed an analytic model for the aggregation of completely coalesced particles undergoing diffusive motion on a surface.[20] The model assumes that the diffusivity depends on size as

$$D(m) = D_0\left(\frac{m}{m_0}\right)^{-\gamma}, \tag{2}$$

where m is cluster mass and γ is a constant. D_0 is defined as $D_0 = D(m_0)$ where m_0 is an arbitrarily chosen reference mass. Kashchiev predicted that the number of particles per unit area $\langle n\rangle$ would depend on time, after sufficiently long time, as

$$\langle n\rangle \propto (D_0 m_0^{\gamma} t)^{-1/(1+\gamma)}. \tag{3}$$

Thus, the density would decrease more slowly with time if the diffusivity decreased more rapidly with size (large particles would have little chance of encountering one another). It is important that an analogous dependence $\langle n\rangle \propto t^{-1/(1+\gamma)}$ was predicted by Kolb for 2D growth.[21]

As suggested by Haley and Weaver,[7] these models for 2D and 3D growth can be applied to BLAG. To confirm this compatibility, we calculated the fractal dimension D_f of ramified islands grown on Xe, Kr, and Ar from the rate of increase of their projected area A with their average radius from the center of mass R: $A \propto R^{D_f}$. Analysis of several thousand islands grown on 30 – 120 ML of Xe, Kr, and Ar yields D_f of 1.72 ± 0.01, 1.70 ± 0.01, and 1.82 ± 0.01, respectively. These values are in fair agreement with Monte Carlo simu-

lations of diffusion-limited cluster-cluster aggregation, which yield $D_f \sim 1.6$–1.7 at the observed surface coverage of 13% – 19% (Ref. 22).

A quantitative connection between Eqs. (1) and (3) requires knowledge of γ and a model that relates θ to both D_0 and t, as developed in the following. It is important to stress, however, that the linear dimensions of the nanostructures grow rapidly in 2D growth and their average radius can become comparable to the nearest-neighbor separation, an effect not considered in theoretical models developed for the dilute limit. Thus, one should not expect Eq. (3) to hold for large ramified structures, such as those for 5 Å Au on 30 or more monolayers.

D. Cluster diffusivities from size distributions: Complete coalescence regime

Analytical models and Monte Carlo simulations have shown that the size distribution takes a universal time-invariant form in systems of diffusing and aggregating particles. This distribution reflects the dependence of diffusivity on size—i.e., Eq. (2).[20,21,23] For 3D aggregation, Kashchiev derived an approximate solution for the normalized size distribution function—namely,

$$\frac{N(r,t)}{N_{max}(t)} = u^{2(3\gamma+1)} e^{-2(3\gamma+1)(u^3-1)/3} \gamma > -1/3, \qquad (4)$$

where $u = r/r_{N_{max}}(t)$. Here $r_{N_{max}}(t)$ is the radius of the particles with the largest population number at a given time and $N_{max}(t)$ is that number. γ is defined in Eq. (2). For $\gamma = 0$, this solution becomes exact because the diffusivity is independent of mass,[20] $D(m) = D_0$, and all particles have a diffusion length of $\langle x^2 \rangle \propto D_0 t$. From Eq. (4), it is clear that the size distribution is independent of the initial size distribution as long as a steady-state process is established. Figure 5(a) shows that the size distributions from Eq. (4) exhibit bell-shaped curves for most values of γ. Most noteworthy, the size distribution narrows with increasing γ, and we can determine γ from the width of experimental size distribution curves. It must be emphasized that the absolute value of γ has a physical meaning only when it is constant (or saturated). Any change of γ during aggregation requires a finite number of aggregation events in order to be reflected in the shape of the size distribution.

To compare BLAG size distributions to Eq. (4), we deposited 1 Å Au onto Xe and Kr buffers of various thicknesses to produce clusters on the buffer with an initial mean radius $\langle r \rangle$ of 1 nm. The final size distribution was measured and normalized to fit Eq. (4). *A priori*, we expected positive values of γ for a given thickness that would indicate reduced diffusivity with increased size. Figures 5(b) and 5(c) show a sample of the experimental results for buffer thicknesses up to 60 ML. The mean sizes $\langle r \rangle$ were measured values, and the solid lines represent fits with Eq. (4) with the values of γ given. Contrary to expectations, the normalized size distributions did not converge to a universal curve, and the values of γ varied significantly.

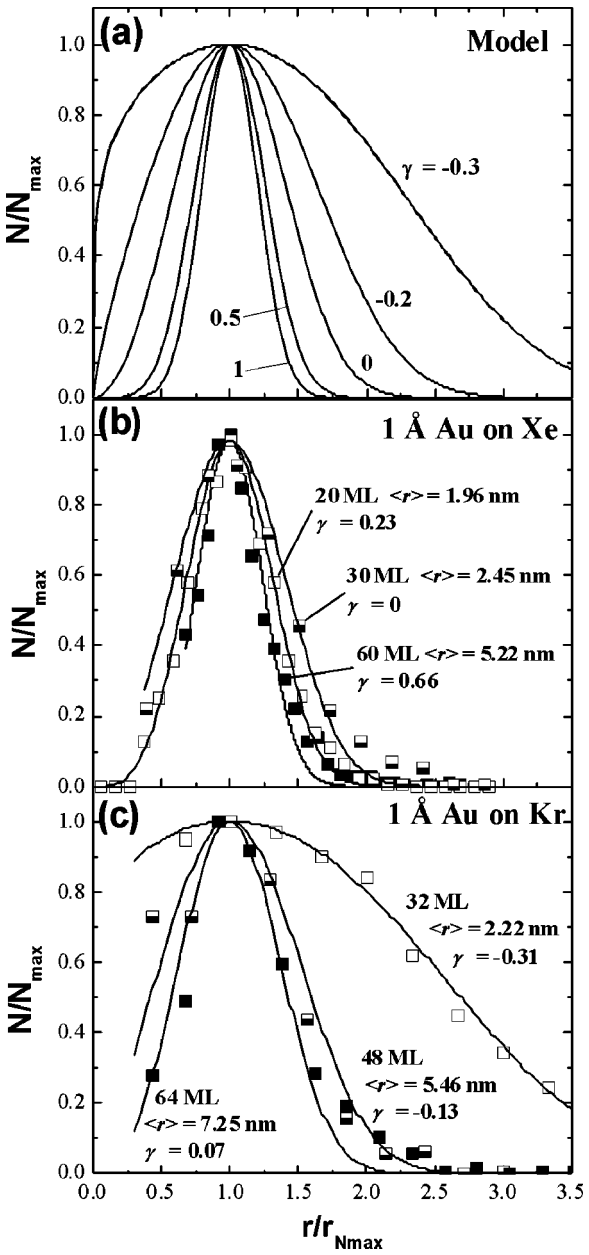

FIG. 5. (a) Size distribution histograms for different values of the parameter γ from Eq. (4) (Ref. 20), showing a broadening with decreasing γ. (b) and (c) show normalized distributions for clusters grown on Xe and Kr with mean radii deduced from experiment and values of γ obtained by best fits of Eq. (4). These results represent compact growth of small structures. The complex behavior of γ indicates activation of diffusion that is unique to these structures—namely, diffusion assisted by energy release during coalescence.

Figure 6 summarizes the intriguing dependence of γ on $\langle r \rangle$ for Xe and Kr buffers, where an increase in $\langle r \rangle$ implies an increase in buffer thickness. A dip at small sizes corresponds to a broadening of the size distribution, and a negative value of γ indicates that the diffusivity increases with size. For larger compact clusters produced by growth on 60 ML Xe [Fig. 2(a)], γ recovers asymptotically to $\sim 2/3$. The importance of this value is that it indicates that cluster diffusivity is proportional to its surface area and, therefore, to its

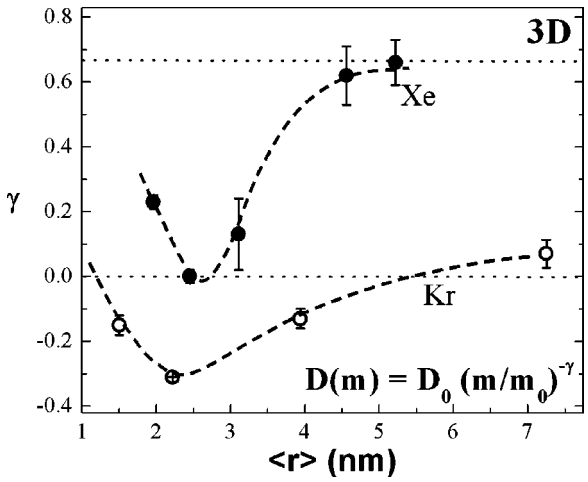

FIG. 6. The evolution of γ with mean cluster size on Xe and Kr buffers. There is a minimum in γ for small clusters, an effect we attribute to heating during coalescence. This effect diminishes with increased size. γ saturates at $\sim 2/3$ for larger clusters on Xe, corresponding to a diffusivity that is inversely proportional to cluster-buffer contact area. The dashed lines are to guide the eye, and the dotted lines mark the physically important values $\gamma=0$ (diffusivity independent of mass) and $\gamma=2/3$.

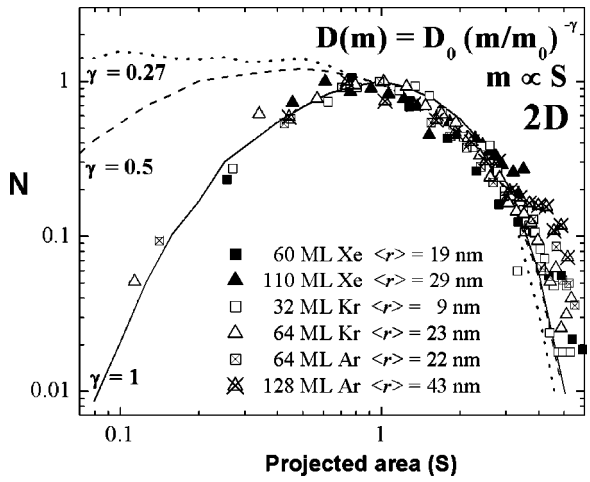

FIG. 7. Experimental size distributions for large ramified islands formed by 2D aggregation following deposition of 5 Å Au on Xe, Kr, and Ar. The projected area S is proportional to the mass so the diffusivity scales as $D(S)=D_0(S/S_0)^{-\gamma}$. The lines corresponding to $\gamma=0.27$, 0.5, and 1 allow comparison to Monte Carlo simulations from Ref. 23. The diffusivity of the islands is well represented by $\gamma=1$. Thus, the diffusivity is inversely proportional to the contact area with the buffer, indicating viscous friction.

contact area with the buffer. Diffusion on Kr produces consistently broader size distributions and smaller values of γ for the same average size. Figure 6 also indicates that cluster diffusivity on Kr increases with size (negative values of γ). For growth on 64 ML Kr, γ approaches ~ 0.07 (weak dependence of diffusivity on size). Note that clusters grown on buffers thicker than ~ 60 ML Xe and ~ 64 ML Kr deviate increasingly from being compact (onset of 2D growth). Hence, the probability of aggregation of two ramified islands depends on the extent of their branches as well as their diffusivity. At this point, analysis based on the theory of Ref. 20 becomes inapplicable.

The unexpected dependence of the diffusivity on size for small compact clusters provides insights into the dynamics of movement that are not found in the assumptions of Ref. 20. In particular, it is important to consider how the energy released during coalescence influences cluster motion, as first suggested by Huang *et al.*[2] For small clusters at a given moment during BLAG, the size distribution curve has a pronounced peak [Fig. 5(b)]. During aggregation, the small-size tail is depleted and the large-size tail augmented, resulting in a shift of the peak. One would expect that the larger a cluster is, the more recently it had been formed. Coalescence releases a considerable amount of energy due to the reduction in surface area, as in Fig. 3(a). This energy would be released as coalescence progresses, and a finite amount of time would be required for dissipation. This can happen either by contributing phonons to the buffer across the highly incommensurate boundary or by forcing buffer-atom desorption, particularly atoms adsorbed on the cluster (adsorption reduces the cluster surface energy). Larger clusters would then be ''warmer'' than their smaller counterparts at any given moment. If the diffusivity is assumed to scale as $e^{-\varepsilon_d/kT}$ (discussed below), this heat would be manifest in increased diffusion. Thus, the size distribution would be broader and γ would appear to be lower. The effect would be greater for Kr than for Xe because the Au-Kr binding energy is smaller [120 vs 170 meV (Ref. 24)], the diffusion barrier would be smaller, and the same temperature increase would translate into a smaller ratio of ε_d/kT. This is indeed what is seen in Fig. 6.[25]

The size distribution of the as-nucleated clusters on Xe [as in Fig. 2(a) for 4 ML] yields $\gamma=0.17$. The onset of aggregation would lead to a widening of the size distribution and a lower γ. As the average size increases, the rate of coalescence decreases[26] and so would the rate of energy release relative to the cluster mass. Thus γ would exhibit a minimum. For large enough structures, the effect of self-heating would be insignificant. This hypothesis is consistent with the observed increase of γ with size when $\langle r\rangle$ exceeds 2 nm and the saturation at $\gamma=2/3$ for $\langle r\rangle\sim 5$ nm on Xe (Fig. 6). According to Eq. (2), this corresponds to diffusivity scaling as the inverse of the cluster surface area (and likewise the contact area with the buffer), which is consistent with the scaling found for large ramified structures, as shown in the next section.

E. Cluster diffusivities from size distributions: Incomplete coalescence regime

For purely 2D cluster-cluster aggregation, there is no analytic expression that relates the cluster size distribution to the diffusivity. However, the problem has been tackled through Monte Carlo simulations by Kolb[21] and Meakin *et al.*[23] Figure 6 in Ref. 23 gives size distribution results for 2D aggregation as a function of area at 5% surface coverage for several values of γ. The results are reproduced in Fig. 7 for $\gamma=0.27$, 0.5, and 1. The simulation predicts that the large-size

TABLE I. Characteristics of Au nanostructure diffusion and aggregation on Ar, Kr, and Xe. The cohesive energies of the rare-gas solids are 95, 120, and 167 meV, respectively, and the lattice constants at 4 K are $a_0 = 6.13$, 5.64, and 5.31 Å. For Au, $a_0 = 4.08$ Å.

Size	Shape	γ	Growth rate
$\langle r\rangle < 5$ nm, $N < 3\times10^4$ atoms	3D compact	γ varies (significant self-heating) coalescence-assisted diffusion	$\langle n\rangle \propto \theta^{-3.2}$
$\langle r\rangle \sim 5$ nm, $N \sim 3\times10^4$ atoms	3D compact	$\gamma \rightarrow \frac{2}{3}$ (minimal self-heating) Diffusivity$\propto \frac{1}{\text{contact area}}$[a]	$\langle n\rangle \propto \theta^{-3.2}$
$\langle r\rangle > 10$ nm, $N > 2\times10^5$ atoms	2D ramified	$\gamma = 1$ (negligible self-heating) Diffusivity$\propto \frac{1}{\text{contact area}}$	$\langle n\rangle \propto \theta^{-2.3}$

[a]For Xe only. For Kr, self-heating is still significant.

tail is essentially independent of γ while the small-size tail depends strongly on γ, and there is a crossover from peaked to monotonically decreasing distribution for values below 0.27.

Figure 7 also shows the size distributions from BLAG on Ar, Kr, and Xe in the 2D coalescence regime. The experimental data define a general behavior for all three buffer species and a wide range of cluster sizes ($\langle r\rangle$ from 9 to 43 nm). Moreover, there is good agreement between experiment and simulation for $\gamma = 1$. We conclude that the diffusivity is inversely proportional to the contact area between the Au nanostructures and the buffer layer, for any buffer composition. This is consistent with the asymptotic behavior of compact clusters on Xe described above. Since the contact area increases more slowly with mass in 3D than in 2D growth, the densities for 1 Å depositions are expected to decrease faster with time according to Eq. (3). This is in qualitative agreement with the experimental slopes in Fig. 4 where the densities are shown to decrease as a function of buffer layer thickness rather than time.

F. Friction at the Au-solid interface

From the above, the motion of Au nanostructures on rare-gas solids is characterized by a diffusion constant D that is inversely proportional to the buffer contact area [$\gamma = 2/3$ for compact and 1 for ramified nanostructures (Table I)]. This is important because Widom and Krim[27] deduced, on the basis of the fluctuation-dissipation theorem, that the diffusivity of thin-film particles spreading on a surface is inversely proportional to the coefficient of its viscous friction with the surface (where viscous implies that the frictional force is proportional to velocity and the contact area of the sliding surfaces). The similarity suggests that particle diffusivity in BLAG is determined by viscous friction with the buffer layer. Thus, cluster mobility is inherently related to the inverted problem of friction of rare-gas solid layers on metal surfaces, which has been studied extensively, both experimentally through quartz microbalance measurements[28–30] and theoretically through molecular dynamics simulations.[31,32]

In BLAG, the nanocrystals slip on van der Waals solids. Insight into motion and friction at such interfaces comes from recent molecular dynamics studies of a similar system in which the clusters and substrate were both van der Waals solids.[9] For an *incommensurate* substrate, the diffusivity was again found to depend inversely on contact area. In this case, the trajectory of the sliding clusters did not reflect the structure of the surface. For a *commensurate* interface, there was a much stronger dependence of D on contact area ($\gamma = 1.4$ for compact clusters). D was deduced to be many orders of magnitude higher for an incommensurate system compared with a commensurate one for a given cluster size. A profound dependence of the force of friction[33] on the lattice match of two semi-infinite sliding surfaces, amounting to more than 10 orders of magnitude, was predicted theoretically by Sokoloff.[34] The simulation by Deltour *et al.* also showed that diffusion was thermally activated, with an effective activation energy for 3D clusters composed of hundreds of atoms that was 1.65 times the single-atom binding energy between cluster and substrate atoms.[35] Cluster and substrate vibration modes were shown to be equally effective in causing motion. This is consistent with our model of enhanced diffusion caused by coalescence though such a source of heat was not considered in the simulations.

G. Mechanism of buffer-layer-assisted growth

Cluster motion is most likely activated by random ''knocks'' from either the buffer phonons or their own lattice vibration modes. In analogy with the results by Deltour *et al.*, the diffusivity can be expected to be thermally activated,

$$D_0(T) = D_{00}\ e^{-\varepsilon_d/kT}, \tag{5}$$

where D_0 is defined in Eq. (2), ε_d is the effective activation energy, and k is the Boltzmann constant. Significantly, the same activation energy should hold for nanostructures with sizes from a few nm to at least hundreds of nm, due to the strong incommensurability of the interface. The role of the rare-gas solid is then to isolate the substrate, to facilitate clustering, and to provide a low-friction interface. Two roles of desorption in BLAG are that (1) that it unlocks cluster motion by removing the top buffer layers, as the clusters may be partially buried,[36] and (2) it limits the temperature and time available for aggregation and coalescence.

From the postulate of thermally activated diffusion [Eq. (5)] and its dependence on cluster size [Eq. (2)] and from Eq. (3), it is possible to fit the observed power law growth by modeling a simplified system in which the contribution from the energy released from coalescence is ignored. In this case,

the density of clusters $\langle n \rangle$ is determined by competition between cluster diffusion and buffer desorption. The desorption rate is

$$dN/dt = Ae^{-\varepsilon_b/kT}, \tag{6}$$

where ε_b is the latent heat of desorption and A is the desorption prefactor.[37] Equations (1) and (3) can be related if we approximate the temperature dependence on time as a linear function $T = T_0 + \beta t$ where β is the rate of temperature increase. The total increase in temperature during buffer desorption is an order of magnitude smaller than the temperature T_0 at which it becomes significant. Hence, $T = T_0(1 + \beta t/T_0) \sim T_0(1 - \beta t/T_0)^{-1}$ and Eq. (6) becomes

$$dN/dt = Ae^{-\varepsilon_b/kT_0} e^{\varepsilon_b \beta t/kT_0^2}. \tag{7}$$

The buffer thickness deposited is $\theta = \int_0^t (dN/dt')dt'$, where t is the total time for desorption of θ monolayers. Solving for t yields a logarithmic dependence on θ:

$$t(\theta) = \frac{kT_0^2}{\varepsilon_b \beta} \ln\left(\frac{\varepsilon_b \beta \theta e^{\varepsilon_b/kT_0}}{AkT_0^2} + 1 \right). \tag{8}$$

Applying the same approximation for the time dependence of temperature [as in Eq. (7)] to Eq. (5) and substituting Eq. (8) in Eq. (5) gives

$$D_0 = D_{00}\ e^{-\varepsilon_d/kT_0} \left(\frac{\varepsilon_b \beta \theta e^{\varepsilon_b/kT_0}}{AkT_0^2} + 1 \right)^{\varepsilon_d/\varepsilon_b}. \tag{9}$$

Substituting Eqs. (8) and (9) for t and D_0 in Eq. (3) yields for the cluster density

$$\langle n \rangle \propto \left[D_{00}\ m_0^{\gamma} e^{-\varepsilon_d/kT_0} \left(\frac{\varepsilon_b \beta \theta e^{\varepsilon_b/kT_0}}{AkT_0^2} + 1 \right)^{\varepsilon_d/\varepsilon_b} \times \frac{kT_0^2}{\varepsilon_b \beta} \ln\left(\frac{\varepsilon_b \beta \theta e^{\varepsilon_b/kT_0}}{AkT_0^2} + 1 \right) \right]^{-1/(1+\gamma)}. \tag{10}$$

The importance of Eq. (10) is that it tells us that most of the contribution of the buffer thickness to nanostructure growth stems from the increase of diffusivity (as a power law of θ) rather than on the increase of time available for diffusion (logarithmic dependence on θ), in agreement with the power law observed in our experiments (Fig. 4).

For Xe buffer layers, a typical warm-up rate was $\beta \sim 3 \times 10^{-2}$ Ks^{-1}, amounting to 5.2 min for desorption of the first 10^2 monolayers of Xe. Moreover, $\varepsilon_b = 0.167$ eV, $A \sim 10^{12}$ s^{-1}, θ was of the order of 10^2 ML, and the temperature at which desorption became significant was $T_0 \sim 60$ K. The first term in the logarithm in Eq. (8) is then of order 10^3 and the additive constant can be ignored. Comparing Eqs. (1) and (10) gives an expression for the slopes of Fig. 4 for 1-Å Au depositions—namely,

$$z = -\frac{\delta + \dfrac{\varepsilon_d}{\varepsilon_b}}{1+\gamma}, \tag{11}$$

where δ is the contribution from the logarithmic term in Eq. (10). In order to estimate δ, we fitted its values for a range of θ to the exponential function θ^{δ} and found that $\delta \sim 0.3$ for Xe and ~ 0.4 for Kr. Hence, the effective activation energy for diffusion can be determined if γ is known. For $\gamma = 2/3$, we obtain $\varepsilon_d = 0.61$ eV for Kr and 0.82 eV for Xe. These values are certainly exaggerated since the effect of energy released from coalescence is ignored. An experimental study to determine the temperature dependence of BLAG, currently underway, will help determine more precisely the effective activation energy for cluster diffusion and its corresponding prefactor.

IV. CONCLUSIONS

We have studied the aggregation and coalescence of clusters grown by physical vapor deposition on Ar, Kr, and Xe as a function of the buffer thickness and amount of Au deposited. Cluster motion during warm-up and buffer desorption accounts for the growth of nanostructures whose average size can change over three orders of magnitude. The normalized size distributions of large ramified islands converged into a single, scale-invariant function, and comparison with Monte Carlo simulations indicates that the diffusivity scales as the inverse of the island surface area. This scaling indicates that diffusion is controlled by friction at the nanoscale contact between a cluster facet and the buffer surface.

The size distributions for compact Au clusters with mean radius below ~ 5 nm were more complex. The breadth of the scaled size distributions reached a maximum at a certain average cluster size, and it was larger for clusters grown on Kr than on Xe (at the maximum, $\langle r \rangle/\sigma = 1.9$ and 2.7, respectively). Analysis based on an analytical model for crystallite aggregation yielded poor agreement. We attribute this to a dynamic effect in which diffusivity is increased by energy release during cluster coalescence. This process is affected by the competition between the rate of energy release and its dissipation through the buffer. With increased cluster size, the diffusivity again scaled as the inverse of surface area.

We proposed a simplified model for the buffer-layer-assisted growth to describe fast thermally activated diffusion on a buffer with a large lattice mismatch. There are two processes that are most important in aggregation. First, the multilayer buffer must desorb, and desorption of thicker layers provides more time. Second, there is an increase in temperature during the desorption period, and this is manifest in the diffusivity as $e^{-\varepsilon_d/kT}$. Competition between the two processes determines the final cluster density and its dependence on the rate of desorption. The model confirms the observed power law growth and yields an upper limit for the effective diffusion activation energy.

ACKNOWLEDGMENTS

This work was supported in part by the U.S. Army Research Office and in part by the US Department of Energy,

Division of Materials Sciences under Grant Nos. DEFG02-01ER45944 and DEFG02-91ER45439 through the Frederick Seitz Materials Research Laboratory. We thank C.M. Aldao, P.S. Waggoner, and Koji S. Nakayama for stimulating discussions. One of the authors (A.S.B.) acknowledges support from the Fulbright Commission and CIES.

*Permanent address: Department of Physics, Quaid-e-Azam Campus, University of the Punjab, Lahore-54590, Pakistan.

[1] P. Jensen, Rev. Mod. Phys. **71**, 1695 (1999).

[2] L. Huang, S. J. Chey, and J. H. Weaver, Phys. Rev. Lett. **80**, 4095 (1998).

[3] G. D. Waddill, I. M. Vitomirov, C. M. Aldao, and J. H. Weaver, Phys. Rev. Lett. **62**, 1568 (1989).

[4] G. D. Waddill, I. M. Vitomirov, C. M. Aldao, S. G. Anderson, C. Capasso, J. H. Weaver, and Z. Liliental-Weber, Phys. Rev. B **41**, 5293 (1990).

[5] See Ref. 2 for growth on Si. See Ref. 4 for growth on GaAs. For growth on high-temperature superconductors, see T. R. Ohno, Y.-N. Yang, G. H. Kroll, K. Krause, L. D. Schmidt, J. H. Weaver, Y. Kimachi, Y. Hidaka, S. H. Pan, and A. L. de Lozanne, Phys. Rev. B **44**, 2430 (1991); T. R. Ohno, Y.-N. Yang, J. H. Weaver, Y. Kimachi, and Y. Hidaka, Appl. Phys. Lett. **57**, 718 (1990).

[6] J. H. Weaver and G. D. Waddill, Science **251**, 1444 (1991).

[7] C. L. Haley and J. H. Weaver, Surf. Sci. **518**, 243 (2002).

[8] V. N. Antonov and J. H. Weaver, Surf. Sci. **526**, 97 (2003).

[9] P. Deltour, J. L. Barrat, and P. Jensen, Phys. Rev. Lett. **78**, 4597 (1997).

[10] A. Zangwill, *Physics at Surfaces* (Cambridge University Press, Cambridge, England, 1988).

[11] M. C. Bartelt, S. Günther, E. Kopatzki, R. J. Behm, and J. W. Evans, Phys. Rev. B **53**, 4099 (1996).

[12] The rare-gas buffer is always solid. The equilibrium melting temperature of Xe is 161 K, and an adsorbed rare-gas monolayer remains crystalline below $0.6\epsilon/k$ [where ϵ is the interatomic potential (Ref. 31)] or 139 K for Xe. At this temperature, the buffer has completely sublimed in our experiments.

[13] Z. L. Wang, J. Phys. Chem. B **104**, 1153 (2000), and references therein.

[14] H. Reiss, J. Appl. Phys. **39**, 5045 (1968).

[15] H. Zhu and R. S. Averback, Philos. Mag. Lett. **73**, 27 (1996).

[16] L. J. Lewis, P. Jensen, and J. L. Barrat, Phys. Rev. B **56**, 2248 (1997).

[17] F. A. Nichols, J. Appl. Phys. **37**, 2805 (1966).

[18] F. A. Nichols and W. W. Mullins, J. Appl. Phys. **36**, 1826 (1965).

[19] The reduction reflects the fact that nearby clusters grow together and that energy released from atom capture can make small clusters mobile.

[20] D. Kashchiev, Surf. Sci. **55**, 477 (1976).

[21] M. Kolb, Phys. Rev. Lett. **53**, 1653 (1984).

[22] St. C. Pencea and M. Dumitrascu, in *Fractal Aspects of Materials* edited by F. Family, B. Sapoval, P. Meabin, and R. Wool MRS Symposia Proceedings No. 367 (Materials Research Society, Pittsburgh), p. 373.

[23] P. Meakin, T. Vicsek, and F. Family, Phys. Rev. B **31**, 564 (1985).

[24] G. Vidali, G. Ihm, H. Y. Kim, and M. W. Cole, Surf. Sci. Rep. **12**, 133 (1991).

[25] The effect should be even more pronounced on Ar. It would be observable if the sample were cold enough to produce a smooth buffer surface. At 20 K, however, Ar buffers have inhomogeneous thicknesses and cluster densities.

[26] A recent study has demonstrated that the relaxation time of shape equilibration increases exponentially with crystallite size [Nicolas Combe, Pablo Jensen, and Alberto Pimpinelli, Phys. Rev. Lett. **85**, 110 (2000)].

[27] A. Widom and J. Krim, Phys. Rev. E **49**, 4154 (1994).

[28] E. T. Watts, J. Krim, and A. Widom, Phys. Rev. B **41**, 3466 (1990).

[29] J. Krim, D. H. Solina, and R. Chiarello, Phys. Rev. Lett. **66**, 181 (1991).

[30] C. Daly and J. Krim, Phys. Rev. Lett. **76**, 803 (1996).

[31] M. Cieplak, E. D. Smith, and M. O. Robbins, Science **265**, 1209 (1994).

[32] E. D. Smith, M. O. Robbins, and M. Cieplak, Phys. Rev. B **54**, 8252 (1996).

[33] In this model, friction was assumed to arise from the excitation of lattice vibration modes during the sliding of the two surfaces.

[34] J. B. Sokoloff, Phys. Rev. B **42**, 760 (1990).

[35] The binding energy of single Xe, Kr, or Ar atoms to polycrystalline Au is within several percent of the cohesive energy of the corresponding rare-gas solid (see Ref. 24).

[36] T. R. Ohno, J. C. Patrin, U. S. Ayyala, and J. H. Weaver, Phys. Rev. B **44**, 1891 (1991).

[37] J. A. Venables, *Introduction to Surface and Thin Film Processes* (Cambridge University Press, Cambridge, England, 2000).